c-Abl tyrosine kinase regulates cardiac growth and development

Zhaozhu Qiu[a], Yong Cang[b,c,1], and Stephen P. Goff[a,b,1]

[a]Departments of Microbiology and [b]Biochemistry and Molecular Biophysics, Howard Hughes Medical Institute, Columbia University College of Physicians and Surgeons, New York, NY 10032; and [c]Burnham Institute for Medical Research, La Jolla, CA 92037

Contributed by Stephen P. Goff, November 23, 2009 (sent for review October 9, 2009)

The c-Abl protein is a ubiquitously expressed nonreceptor tyrosine kinase involved in the development and function of many mammalian organ systems, including the immune system and bone. Here we show that homozygous *Abl* mutant embryos and newborns on the C57BL/6J background, but not on other backgrounds, display dramatically enlarged hearts and die perinatally. The heart defects can be largely rescued by cardiomyocyte-specific restoration of the full-length c-Abl protein. The cardiac hyperplasia phenotype is not caused by decreased apoptosis, but rather by abnormally increased cardiomyocyte proliferation during later stages of embryogenesis. Genes involved in cardiac stress and remodeling and cell cycle regulation are also up-regulated in the mutant hearts. These findings reveal an essential role for c-Abl in mammalian heart growth and development.

Abelson | heart development | hyperproliferation

Organ formation during embryogenesis is an intricate process in which multipotent progenitor cells commit to specific lineages and multiple differentiated cell types interact and organize into a precise 3-dimensional structure. To generate and maintain the proper size and shape of the mature organ, cell proliferation and differentiation need to be tightly regulated. The molecular mechanisms responsible for this delicate balance are complicated and remain poorly understood in many settings.

Cardiac ventricular chamber formation involves regulated cardiomyocyte proliferation and dynamic changes in myocardial architecture, including trabeculation and thickening of the initial compact layer (1–3). The inner trabeculae in mouse hearts, which contain highly organized muscular ridges lined by endocardial cells, form as a result of interactions between primitive myocardium and endocardium over the time period from embryonic day (E) 9.5 to E13.5. The outer compact myocardium, distributed along the ventricular wall, is more mitotic and less differentiated than trabecular myocardium at this time. As morphogenesis of the ventricle progresses, the overall proliferative activity of cardiac progenitor cells gradually declines and is completely terminated soon after birth (4, 5). How cardiac proliferation is regulated during later stages of embryogenesis is largely unknown. In particular, what triggers cardiomyocytes to withdraw from the cell cycle at birth is still unclear.

c-Abl is a ubiquitously expressed nonreceptor tyrosine kinase implicated in the regulation of cell proliferation, survival, and migration (6). c-Abl and its close relative Arg (i.e., Abl-related gene) share similar SH3, SH2, and tyrosine kinase domains with other Src-family members but, in addition, contain a unique large carboxyl-terminal fragment with multiple functional domains including proline-rich sequences, nuclear localization signals (NLSs), actin-binding domains and a nuclear export signal. Disruption of *Abl* in mice on a mixed genetic background results in neonatal lethality accompanied by pleiotropic developmental defects with variable penetrance, including runting, splenic and thymic atrophy, B cell lymphopenia, dysfunctional osteoblasts, and foreshortened crania (7–9). Recent evidence also suggests a possible connection between c-Abl and heart development and physiology. It has been shown that the transmembrane semaphorin Sema6D signaling, likely mediated by c-Abl, promotes the migration of myocardium into the trabeculae in chicken embryos (10). In humans and mice, the cancer therapeutic agent imatinib (Gleevec; Novartis), a small-molecule tyrosine kinase inhibitor, was reported to cause left ventricular contractile dysfunction and dilation (11). Analysis of isolated cardiomyocytes from mice that had received imatinib revealed mitochondrial abnormalities, activation of the endoplasmic reticulum stress response, and consequent cell death. It is believed that imatinib-induced cardiotoxicity is mediated by inhibition of endogenous c-Abl. However, there remains no direct evidence of a role for c-Abl in mammalian cardiac growth and development. In this study, we report a previously unappreciated critical function for c-Abl in regulating cardiomyocyte proliferation during late mouse gestation. This finding not only reveals an unanticipated aspect of c-Abl biology, but also has implications for the possible side effects of imatinib on fetal cardiac development (12).

Results

Severe Perinatal Lethality of *Abl* Mutant Mice on C57BL/6J Background. To introduce an *Abl* knockout (KO) mutation into defined genetic backgrounds, we backcrossed Abl^2 (an *Abl*-null allele) heterozygous animals with 129/SvEv (129) and C57BL/6J (B6) inbred mice for more than 10 generations. Homozygous *Abl* KO animals were then generated by intercrossing heterozygous mice of the specific backgrounds. At postnatal day (P) 14, approximately 50% of the expected homozygous *Abl* mutant 129 or 129xB6 mice were viable, consistent with previous observations (8, 9) (Table 1). However, on the B6 background, only 4% (1 of 28) of the expected homozygous *Abl* mutant mice survived at P14. Approximately 90% of these mice died between P0 and P1. In contrast, only 10% of the homozygous *Abl* KO 129xB6 mice were dead at birth (Table 1). Analysis of offspring from timed matings of heterozygous mutant B6 mice revealed $Abl^{-/-}$ embryos between E14.5 and E18.5 surviving at a frequency slightly less than the expected Mendelian ratio, with occasional dead and degenerating mutant embryos (Table 1). These data suggest that loss of c-Abl in mice on the B6 background causes a more severe phenotype than on a mixed background, with a high mortality rate between E18.5 and P1.

To rule out the possibility that the high perinatal lethality on the B6 background was caused by other spontaneous mutations arising in the course of the backcrossing, we also examined the effect of genetic background on another *Abl* mutant allele: Abl^{m1}. Unlike the null allele Abl^2, Abl^{m1} eliminates only the carboxyl-terminal third of the c-Abl protein and replaces it with neomycin sequences (8). However, it is known that the phenotypes of Abl^2 and Abl^{m1}

Author contributions: Z.Q., Y.C., and S.P.G. designed research; Z.Q. and Y.C. performed research; Z.Q. and Y.C. analyzed data; and Z.Q., Y.C., and S.P.G. wrote the paper.

The authors declare no conflict of interest.

Freely available online through the PNAS open access option.

[1]To whom correspondence may be addressed. E-mail: spg1@columbia.edu or ycang@burnham.org.

This article contains supporting information online at www.pnas.org/cgi/content/full/0913131107/DCSupplemental.

Table 1 Effect of genetic background on perinatal survival of Abl KO mice

Age	Genetic background	Total mice	Expected mutants*	Viable mutants (% of expected)
P14	129xB6	97	24	12 (50)
	B6	112	28	1 (4)
P1	129xB6	81	20	18 (90)
	B6	98	25	2 (8)
E18.5	B6	85	21	18 (86)
E14.5	B6	44	11	10 (91)

**Abl* homozygous mutants were produced by intercrossing heterozygous animals on different backgrounds. The number of expected mutants was estimated based on Mendelian ratio.

mutant mice on a mixed background are indistinguishable (8, 9). Abl^{m1} B6 mice were generated through independent multigenerational backcrossing to inbred B6 animals. Similar to Abl^{2} null animals, Abl^{m1} homozygous mice also exhibited approximately 90% perinatal mortality on the B6 background (Table S1). This suggests that the perinatal lethality phenotype observed in *Abl* mutant animals is indeed a result of loss of c-Abl function.

Cardiac Abnormalities in $Abl^{-/-}$ Mice. To probe the cause(s) of perinatal lethality in the Abl^{2} KO B6 mice, we performed a comprehensive histological analysis of WT and $Abl^{-/-}$ embryos and newborns. These surveys revealed no gross defects in the brain, lung, or liver. However, the hearts of mutant mice displayed dramatic morphological abnormalities of both ventricles and atria (Fig. 1 *A* and *C*). As shown in Fig. 1*A*, most *Abl* KO embryos at E18.5 displayed enlarged ventricles and dilated atria when compared with WT controls. The heart weight–to–body weight ratio in the mutant embryos was approximately 30% higher than in WT littermates (5.87 mg/g ± 0.24 vs. 4.64 mg/g ± 0.19; $P < 0.003$; Fig. 1*B*). More strikingly, histological serial sectioning of the mutant hearts revealed an almost complete disappearance of the 2 ventricular lumens in all *Abl* KO newborns that died at P0 (Fig. 1*C*). Furthermore, the interventricular septum was also thickened in the mutant hearts. Histological analysis of embryos at E18.5 showed expansion of both the trabecular and compact layers of the 2 ventricles (Fig. 1*C*). The early development of *Abl* mutant hearts appeared to be normal as revealed by sectioning of embryos at E14.5 (Fig. 1*C*). Together, these observations indicate that the phenotype of the abnormally enlarged hearts in c-Abl–deficient mice develops during late gestation and peaks at birth. This correlates well with the timing of death of these mutant animals and suggests that severe cardiac defects might be the primary cause of death. In contrast, the hearts of *Abl* null mice on the 129xB6 mixed background, including those that died perinatally and neonatally, were grossly normal compared versus those of WT controls upon histological examination (Fig. 1*C*). This indicates that the involvement of c-Abl in cardiac development is susceptible to modification by the mouse strain background.

High-resolution light microscopy analysis of $Abl^{-/-}$ hearts at E18.5 and P0 revealed that the dramatic increase in organ size was largely caused by an increase in cardiomyocyte cell number rather than cardiac hypertrophy (Fig. 1*D*). It was apparent that, unlike the well organized muscle fibers and smooth oval-shaped nuclei observed in WT mice, the orientation of muscle fibers and the shape of nuclei in *Abl*-null mice were highly irregular (Fig. 1*D*). More nuclei in the mutant hearts also appeared to undergo mitosis (supported by phospho-histone H3 staining; as described later). Furthermore, the KO hearts exhibited increased interstitial space between cardiomyocytes in the trabecular layer, but Masson trichrome staining showed no evidence of fibrosis (Fig. S1). This suggests that the mutant hearts were in the early stage of cardiac remodeling (13). Transmission electron microscopy analysis of E18.5 embryonic hearts from WT and *Abl*-KO mice revealed that mitochondria were randomly distributed, and large hollow mitochondria characterized by loss of vesicles and cristae were evident in the mutant tissues (Fig. 1*E*). In addition, some sarcomeres in the mutant cardiomyocytes were also fragmented and disorganized with abnormal Z-discs (Fig. 1*E*).

Given the severe morphological defects of $Abl^{-/-}$ hearts, we examined several fetal genes that are typically associated with a cardiac stress response by real-time PCR, including those encoding atrial natriuretic peptide (*Nppa*), brain natriuretic peptide (*Nppb*), β-myosin heavy chain (*βMHC*; *Myh7*), and smooth muscle α-actin (*Acta2*). We found all but *Acta2* to be significantly up-regulated in E18.5 *Abl* KO hearts compared with WT controls, a strong indication of cardiac volume overload (Fig. 1*F*). Furthermore, α-myosin heavy chain (*αMHC*; *Myh6*) was down-regulated by approximately 30%, consistent with the shift of myosin heavy chain isoform expression from the adult form (*αMHC*) to the fetal form (*βMHC*) as seen in failing mouse hearts (14).

Increased Cardiomyocyte Proliferation in $Abl^{-/-}$ Mice. To investigate the basis for cardiac hyperplasia in Abl^{2} KO B6 mice, we analyzed cardiomyocyte apoptosis by TUNEL assay. c-Abl is known to promote apoptosis of several types of cells exposed to genotoxic stress or oxidative stress, and its loss could have resulted in increased cardiomyocyte survival during development (6, 15). TUNEL staining revealed a very low level of apoptosis (approximately 1 apoptotic cardiac cell/20× field) in both WT and mutant embryonic hearts at E18.5 (Fig. 2*A*). This suggests that cardiac hyperplasia in *Abl* KO mice is not a result of reduced apoptosis, but is instead caused by elevated cell proliferation.

Cardiac progenitor cells gradually lose their proliferative capacity during later stages of embryogenesis and begin to withdraw from the cell cycle at birth (4, 5). To determine whether cardiac hyperplasia of *Abl* mutants was associated with abnormal cell cycle regulation during late gestation, we scored the prevalence of BrdU incorporation (indicator of S phase) and phosphorylation of histone H3 (indicator of M phase) in E18.5 WT and $Abl^{-/-}$ embryonic hearts (Fig. 2 *B–F*). Compared with those from control littermates, ventricular cardiac tissues from *Abl* KO embryos demonstrated a 1.6-fold increase in BrdU-positive cells (20.1 ± 1.1% vs. 12.7 ± 0.6%; $P < 0.002$) and a 1.9-fold increase in phospho-histone H3 (p-H3)–positive cells (16.0/10× field ± 2.1 vs. 8.3/10× field ± 0.9; $P < 0.02$). Elevated BrdU- and p-H3-positive cells were observed throughout both ventricles and the interventricular septum. Although modest, these increases could readily account for tissue hyperplasia observed in the mutant hearts. High-resolution microscopy of tissue sections costained with p-H3 and cardiac myosin heavy chain (MHC) antibodies confirmed that increased mitosis in mutant hearts was primarily confined to cardiomyocytes, rather than cardiac fibroblasts or endothelial cells (Fig. 2*E*). Increased proliferative activity was not observed in any other tissue examined, including brain, lung, liver, and skeletal muscle. Collectively, these data establish that loss of c-Abl results in increased cardiac proliferation during late gestation.

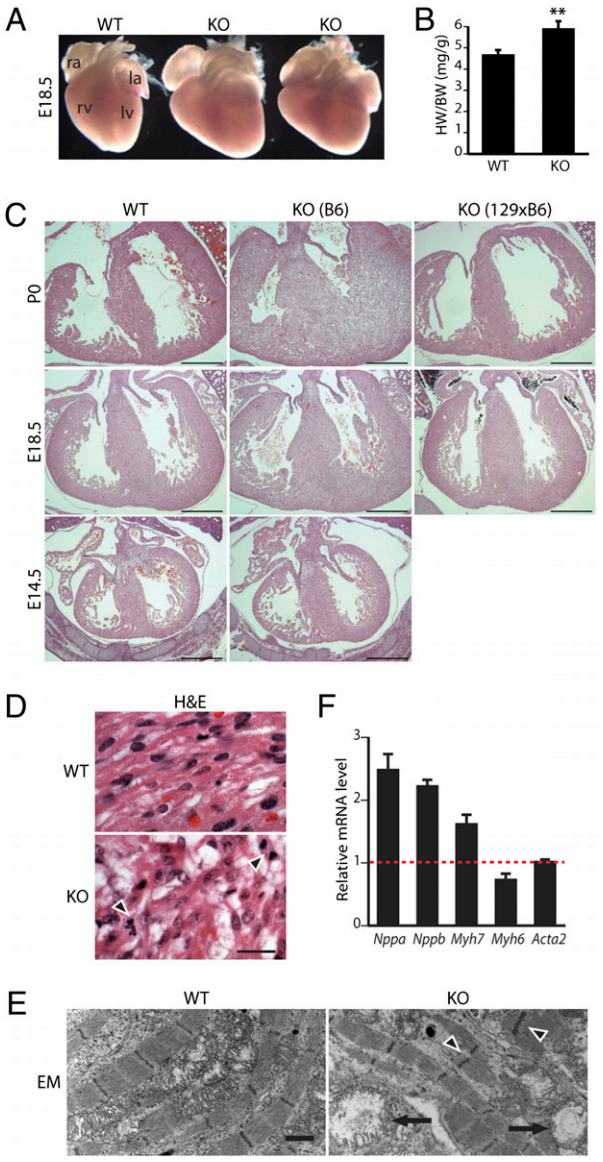

Fig. 1. Cardiac abnormalities in $Abl^{-/-}$ B6 mice. (*A*) Pictures of whole hearts dissected from WT and *Abl* KO embryos at E18.5. Note the enlargement of both ventricles and atria in mutant hearts. (*ra*, right atrium; *la*, left atrium; *rv*, right ventricle; *lv*, left ventricle.) (*B*) Increased heart weight–to–body weight ratio (*HW/BW*) of E18.5 *Abl* KO embryos. The weight of whole ventricular tissues was measured as a function of body weight ($n = 6$ for each genotype; $^{**}P < 0.003$, error bars represent SEM). (*C*) H&E transverse sections of hearts from WT, *Abl* KO B6, and *Abl* KO 129xB6 mice at different developmental time points. Note the gradual thickening of ventricular walls and interventricular septum during the perinatal stage in mutant B6 mice and normal heart morphologies in mutant 129xB6 mice. (Scale bar, 500 μm.) (*D*) H&E transverse sections of P0 WT and *Abl* KO hearts at high magnification showing disorganized muscle fibers and irregularly shaped nuclei in *Abl* KO mice. Arrowheads indicate mitotic nuclei. (Scale bar, 30 μm.) (*E*) Transmission electron micrographs of E18.5 WT and *Abl* KO hearts showing mitochondrial abnormalities and fragmented sarcomeres in mutant hearts. Arrows indicate hollow mitochondria and arrowheads indicate defective Z-discs. (Scale bar, 1 μm.) (*F*) Expression of cardiac genes in E18.5 WT and *Abl* KO hearts measured by real-time PCR. mRNA levels for each gene in mutant hearts were normalized to *Gapdh* and compared with WT hearts ($n = 3$ for each genotype; error bars represent SEM).

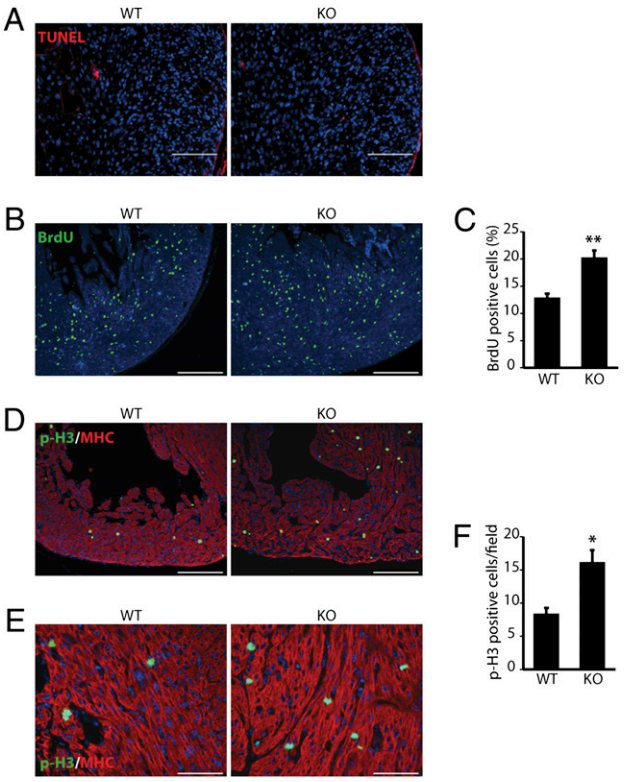

Fig. 2. Increased proliferation in $Abl^{-/-}$ hearts. (*A*) TUNEL assay (red) and DAPI (blue) staining of WT and mutant ventricular sections showing normal apoptosis in *Abl* KO hearts at E18.5. (Scale bar, 100 μm.) (*B*) BrdU (green) and DAPI (blue) staining of WT and mutant left ventricular sections showing increased BrdU incorporation in *Abl* KO hearts at E18.5. (Scale bar, 200 μm.) (*C*) Quantification of BrdU-positive cells was performed on 8 ×60 magnification fields and expressed as a percentage of total cells ($n = 4$ for each genotype; $^{**}P < 0.002$; error bars represent SEM). (*D* and *E*) Phospho-histone H3 (*p-H3*; green), cardiac MHC (red), and DAPI (blue) staining of WT and mutant right ventricular sections showing increased cardiomyocyte proliferation in E18.5 *Abl* KO embryos. (Scale bars, 200 μm in *D*, 67 μm in *E*.) (*F*) Quantification of p-H3–positive cells was performed on 5 ×10 magnification fields (*D*) and expressed as positive cells/field ($n = 4$ for each genotype; $^{*}P < 0.02$, error bars represent SEM).

Cardiomyocyte-Specific Restoration of the Full-Length c-Abl Protein Rescues the Cardiac Hyperplasia Phenotype in Abl^{m3} Mutant Mice. The carboxyl-terminal half of c-Abl, encoded by exon 11, contains 3 NLSs and one nuclear export signal, which drive its nucleo-cytoplasmic shuttling (6). DNA-damaging agents promote nuclear translocation of c-Abl and activated nuclear c-Abl has a proapoptotic function (15). To probe the role of the first NLS (NLS1) in vivo, we introduced an *Abl* mutant allele, containing a mutated NLS1 (5 amino acid substitutions of Lys to Gln) (16) and a neomycin (*neo*) resistance cassette flanked by 2 loxP sites, into B6 embryonic stem (ES) cells through homologous recombination (Fig. 3*A*). Surprisingly, Western blot analysis showed that the mutant allele expressed barely detectable levels of full-length c-Abl protein and only low levels of a fragment consisting of its N-terminal half (Fig. 3 *B* and *C*). Subsequent analysis of cDNA from this line revealed the presence of 2 mRNAs with decreased abundance: one apparently of normal structure, and the other formed by joining exon 10 to a portion of the *neo* cassette, and then to exon 11, encoding a truncated protein (Fig. 3*A* and Fig. S2). These mutant B6 mice exhibited high perinatal mortality with abnormally enlarged hearts, and were phenotypically indistinguishable from *Abl*-null mice (Fig. 3*E*). We named this allele Abl^{m3}. When Abl^{m3} mice were bred to transgenic lines expressing a ubiquitous Cre recombinase (*EIIa-Cre*) to excise the *neo* cassette, the resulting Abl^{nls1} homozygous mice were viable and grossly normal. Western blot analysis of

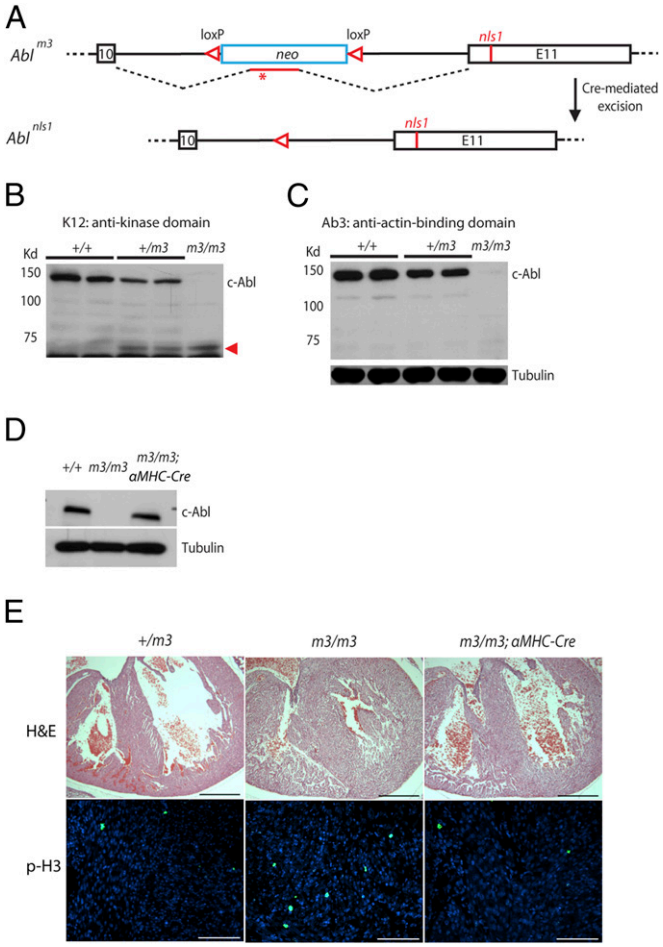

Fig. 3. Cardiac hyperplasia in Abl^{m3} mutant mice rescued by cardiomyocyte-specific expression of full-length c-Abl. (*A*) Scheme of the genomic structures of Abl^{m3} and Abl^{nls1} alleles. The NLS1 mutation was introduced along with a neomycin resistance cassette flanked by loxP sites (red triangles) between exon 10 and exon 11. An abnormal splicing event incorporating a portion of the *neo* cassette with a stop codon (red star) in Abl^{m3} allele is shown in dashed lines. Cre-mediated excision removes the *neo* cassette. (*B* and *C*) Western blot of brain extracts from embryos of the indicated genotypes using 2 different c-Abl antibodies recognizing kinase domain (*K12*; *B*) and C-terminal actin-binding domain (*Ab3*; *C*), respectively. Red arrowhead indicates the N-terminal half of c-Abl expressed by Abl^{m3} mutant allele. (*D*) Western blot of E18.5 heart extracts showing the restoration of full-length c-Abl protein in $Abl^{m3/m3}$; *αMHC-Cre* mice. (*E*) H&E (*Top*) and p-H3 staining (*Bottom*) of heart transverse sections from newborns of the indicated genotypes. [Scale bars, 500 μm (*Top*) and 100 μm (*Bottom*)].

extracts from $Abl^{nls1/nls1}$ mouse embryonic fibroblasts (MEFs) showed restoration of a full-length c-Abl protein with the same nucleo-cytoplasmic distribution as in WT MEFs (Fig. S3). Thus, although the full-length protein retains the mutated NLS1, the mutation does not appear to affect c-Abl steady-state localization. Further study demonstrates that this NLS1 is also dispensable for DNA damage-induced c-Abl nuclear import and apoptosis, suggesting that the trafficking of the mutant protein is still normal (Fig. S3).

To determine whether cardiac hyperplasia of mutant mice deficient in c-Abl was due to a cardiomyocyte-autonomous function of c-Abl, we took advantage of the unique Abl^{m3} mutants and bred them to transgenic B6 mice expressing Cre under the control of the *αMHC* promoter (17), which is specifically expressed in differentiated cardiomyocytes from the embryonic stage. Western blot analysis of cardiac extracts from $Abl^{m3/m3}$; *αMHC-Cre* E18.5 embryos confirmed the efficient restoration of the full-length c-Abl protein to WT control levels (Fig. 3*D*). Histological analysis of $Abl^{m3/m3}$; *αMHC-Cre* newborn hearts showed that both the ventricular walls and interventricular septum were significantly thinner compared with those in $Abl^{m3/m3}$ littermates, although still slightly thicker than those in $Abl^{+/m3}$ controls (Fig. 3*E*). As a result, the 2 ventricular lumens were dramatically expanded in $Abl^{m3/m3}$; *αMHC-Cre* mice. The decreased proliferation in $Abl^{m3/m3}$; *αMHC-Cre* cardiac tissues was also confirmed by p-H3 staining (Fig. 3*E*). These data indicate that c-Abl inhibits proliferation in differentiated cardiomyocytes. Surprisingly, even though the cardiac overproliferation phenotype was largely rescued by c-Abl expression in cardiomyocytes, most $Abl^{m3/m3}$; *αMHC-Cre* pups still died shortly after birth, suggesting that other defects besides cardiac hyperplasia caused death of these mutants. However, we were unable to identify any obvious abnormalities in other organs of $Abl^{m3/m3}$; *αMHC-Cre* mice through a histological survey.

Abnormal Gene Expression in $Abl^{-/-}$ Hearts. In further efforts to identify possible molecular defects in Abl^{2} KO hearts, we compared the gene expression profiles of E17.5 WT and $Abl^{-/-}$ hearts by microarray analysis. At this stage, mutant hearts exhibited relative minor morphological defects. Numerous gene transcripts showed modest changes (within ±3 fold) in $Abl^{-/-}$ hearts (Table S2). Many of the up-regulated genes encode signaling molecules. Real-time PCR analysis of a subset of the up-regulated genes validated approximately half of those examined, suggesting that the subtle changes in the expression of many regulatory genes may contribute to the cardiac abnormalities observed in *Abl* mutant mice (Fig. 4*A*).

We observed a twofold increase in the expression of cardiac ankyrin repeat domain 1 (*Ankrd1*) and insulin-like growth factor binding protein 3 (*Igfbp3*) mRNAs in *Abl* KO hearts using real-time PCR. These 2 genes are associated not only with the cardiac stress response, but also with fetal cardiomyocyte proliferation (18, 19). Furthermore, *Abl* mutant hearts showed a slight increase in expression of mRNAs involved in cardiac cell cycle control, including cyclin D1 (*Ccnd1*) and cyclin D2 (*Ccnd2*), consistent with elevated cardiomyocyte proliferation in these mice. In line with effects of the mutations on cardiac remodeling, 2 major growth factors involved in tissue remodeling and angiogenesis—connective tissue growth factor (*Ctgf*) and vascular endothelial growth factor A (*Vegfa*)—were also up-regulated. Elevated expression of cyclin D1 and CTGF in KO hearts was also confirmed by Western blot analysis of cardiac extracts from E18.5 embryos (Fig. 4*B*). CTGF is known to play a key role in the process of cardiac fibrosis through stimulating extracellular matrix production, including various types of collagens (20). Consistently, immunohistochemical analysis of ventricular sections revealed increased deposition of type I collagen between cardiomyocytes in E19.5 $Abl^{-/-}$ hearts compared with that in control littermates (Fig. 4*C*).

Discussion

In summary, we uncovered a physiological function for c-Abl in mammalian heart growth and development. Loss of c-Abl in B6 mice leads to severe cardiac hyperplasia, which contributes to high lethality around the time of birth. The phenotype is dependent on mouse genetic background, as mutant mice deficient of c-Abl protein on several other backgrounds do not show the similar defects and survive much longer. This indicates that the function of c-Abl in cardiac development is subject to modification from other gene(s) in the mouse genome. The situation is similar to that in Drosophila, in which genetic screens have identified a host of Abl modifier genes that either enhance or suppress the phenotype of D-Abl-null animals (21, 22). For example, mutations in *D-Abl* have no obvious effects on the morphology of the embryonic CNS, and the mutant animals

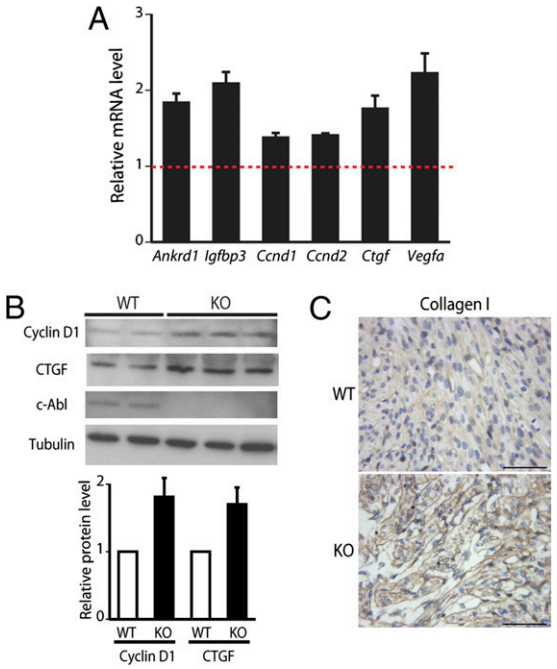

Fig. 4. Aberrant gene expression in $Abl^{-/-}$ hearts. (*A*) Expression of indicated genes in E17.5 WT and *Abl* KO hearts measured by real-time PCR. mRNA levels for each gene in mutant hearts were normalized to *Gapdh* and compared with WT hearts ($n = 3$ for each genotype; error bars indicate SEM). (*B*) Expression of cyclin D1 and CTGF in E18.5 WT and *Abl* KO hearts detected by Western blot (*Top*). Protein levels for each gene (*Bottom*) in mutant hearts were normalized to α-tubulin and compared with WT hearts ($n = 2$ for WT, 3 for KO; error bars indicate SEM). (*C*) Immunohistochemistry analysis of WT and mutant ventricular sections showing increased type I collagen deposition in E19.5 *Abl* KO hearts. (Scale bar, 100 μm.)

survive to the pupal and adult stages; however, flies with homozygous mutations in both *D-Abl* and *Disabled* fail to develop any axon bundles in the CNS and die at the embryonic and early larval stages (21). Therefore, it is likely that specific gene allele(s) in the B6 mouse genome can similarly sensitize heart development to mutations in *Abl*. It will be of interest to identify such modifier gene(s) in future studies.

We show that cardiac hyperplasia observed in *Abl* KO mice is caused by increased cardiac proliferation during late gestation and can be largely rescued by cardiomyocyte-specific c-Abl expression. c-Abl has long been implicated as a negative regulator of cell growth, as overexpression of c-Abl in fibroblasts induces cell cycle arrest in G1 phase (16, 23, 24). However, it has been unclear whether endogenous c-Abl plays a role as a true growth inhibitor because previous studies of *Abl* mutant mice have failed to demonstrate any positive effect of c-Abl deficiency on cell growth (8, 9). On the contrary, in other settings c-Abl activation has been shown to stimulate cell proliferation (25–27). Here we provide in vivo evidence suggesting that c-Abl acts as a key negative regulator of cardiomyocyte proliferation during later stages of embryogenesis. These findings highlight the multifaceted role of c-Abl in regulating cell proliferation, which is dependent on specific cell types and developmental stages.

The mechanisms by which loss of c-Abl leads to excessive cardiac proliferation are still uncertain. Cyclin D family members have been shown to play a specific role in promoting cardiomyocyte cell cycle progression (28–30). Elevated expression of cyclin D1 and cyclin D2 may partially explain the overgrowth phenotype in *Abl* mutant hearts. But their increases are relatively modest, and it is certainly not the only possible mechanism (Fig. 4 *A* and *B*). A recent study reports that ephrinB2-EphB4 signaling inhibits breast cancer cell proliferation and migration in vivo (31). These effects are mediated by activation of c-Abl and tyrosine phosphorylation of the adaptor protein Crk, which likely leads to inhibition of Rac1 GTPase activity. EphrinB2-EphB4 signaling is also involved in ventricular trabeculation during early cardiogenesis (32), but the early lethality of their KO embryos at E11 precludes the analysis of its role in late cardiac development.

In conclusion, our data based on studies in mutant mice show that the c-Abl tyrosine kinase negatively regulates cardiac growth during the late stages of heart morphogenesis. The findings thus raise concerns that exposure to c-Abl inhibitors, as previously suggested (12), might similarly affect fetal heart development.

Materials and Methods

Mice. Abl^{m1} and Abl^{2} mice used in the study have been previously reported (8, 9). Homozygous *Abl* mutant mice and embryos were produced by intercrossing heterozygous parents. The day on which the vaginal plug was observed was designated as E0.5. Abl^{m3} targeting vector includes exon 11 with the NLS1 mutation, and a *neo* cassette flanked by loxP sites in the intron between exon 10 and 11. The 5′ arm and 3′ arm of the targeting construct correlate to a 2.4-kb fragment harboring exons 9 to 10, and a 7.2-kb fragment covering the rest of exon 11, respectively. The linearized targeting construct was electroporated into albino B6-derived ES cells. ES cell clones were isolated and analyzed for homologous recombination by Southern analysis. Two properly targeted clones were injected into B6 blastocysts, and 2 resulting male chimeras were crossed to albino B6 females to achieve germline transmission of the targeted allele. Abl^{m3} mice were mated with 2 *Cre* lines: *EIIa-Cre* (JAX 3724) and *αMHC-Cre* (17), a gift of Ira Goldberg (New York, NY). All animal procedures were approved by the Columbia University Institutional Animal Care and Use Committee.

Histology. Embryos were fixed in neutral buffered 10% formalin (Sigma) at 4°C overnight, embedded in paraffin, and sectioned at 5-μm intervals. H&E and Masson trichrome stains were applied according to standard procedures.

Transmission Electron Microscopy. Embryonic hearts were dissected and immediately fixed with 2.5% glutaraldehyde in 0.1M Sorenson buffer (pH 7.2). Samples were processed by the Columbia University Medical Center Electron Microscope Facility. The sections were examined under a Jeol JEM-1200 EXII electron microscope.

Immunofluorescence. The sections were dewaxed and rehydrated, and incubated with primary antibodies against phospho-histone H3 (ab5176; 1:400; Abcam), cardiac myosin heavy chain (ab15; 1:400; Abcam) and type I collagen (ab34710; 1:600; Abcam). Secondary antibodies conjugated with Alexa Fluor (Invitrogen) or HRP (Vector Laboratories) were then applied. TUNEL assay was performed according to the kit instruction (Roche). Slides were mounted with Vectashield mounting medium with DAPI (Vector Laboratories).

BrdU Incorporation and Staining. Time-pregnant females were intraperitoneally injected with BrdU (50 mg/kg body weight; Sigma). Embryos were dissected 1 h after injection. For staining, sections were incubated with 2 N HCl for 30 min at 37°C and then with BrdU antibody (ab6326; 1:200; Abcam).

Real-Time PCR. Total RNA from ventricular tissue was extracted using TRIzol reagent (Invitrogen) and treated with DNase I (Roche). For real-time PCR, total RNA was reverse-transcribed with random hexamers using the SuperScript III First-Strand cDNA Synthesis System (Invitrogen) to synthesize cDNA. cDNA samples were then used as templates for real-time PCR, which was performed on a 7500 Real-Time PCR System (14) with FastStart SYBR Green Master with Rox (Roche). Primer sequences are available upon request. Gene expression was normalized to *Gapdh* and calculated as relative fold change.

Western Blot. Ventricular tissue was homogenized in lysis buffer (20 mM Tris, pH 7.5, 150 mM NaCl, 2 mM EDTA, 1% Nonidet P-40) supplemented with protease inhibitors (Roche). After centrifuging at 15,000 × *g* for 15 min, supernatant was recovered and protein concentration was determined by the Bio-Rad protein assay. Equal amounts were resolved on a 10% SDS/PAGE gel and analyzed by Western blot using a standard protocol. Primary antibodies against c-Abl [K12; 1:1,000 (Santa Cruz Biotechnologies) and Ab3; 1:1,000 (Calbiochem)], cyclin D1 (sc-753; 1:500; Santa Cruz Biotechnologies), CTGF (ab6992; 1:2,000; Abcam), and α-tubulin (T6199; 1:5,000; Sigma) were applied. Band intensity was quantified by densitometry using ImageJ

(National Institutes of Health). Protein expression level was normalized to α-tubulin and calculated as relative fold change to WT samples.

Statistical Analysis. Statistics were calculated with Excel. Statistical significance was assessed by an unpaired Student two-tailed *t* test. Values were considered statistically significant at $P < 0.05$.

ACKNOWLEDGMENTS. We thank Sharon Boast and Jeff Hardin for mice backcrossing, Ira Goldberg for *αMHC-Cre* line, the histology service facility at Columbia University for support, Ramon Diaz Trelles and Mark Mercola for valuable suggestions, as well as Susan Steinberg, Daniel Wolf, and J. Robert Hogg for comments on the manuscript. This work was supported by Grant P01 CA 023767 from the National Cancer Institute. S.P.G. is an Investigator of the Howard Hughes Medical Institute.

1. Sedmera D, Pexieder T, Vuillemin M, Thompson RP, Anderson RH (2000) Developmental patterning of the myocardium. *Anat Rec* 258:319–337.
2. Srivastava D (2006) Making or breaking the heart: from lineage determination to morphogenesis. *Cell* 126:1037–1048.
3. Olson EN (2006) Gene regulatory networks in the evolution and development of the heart. *Science* 313:1922–1927.
4. Pasumarthi KB, Field LJ (2002) Cardiomyocyte cell cycle regulation. *Circ Res* 90: 1044–1054.
5. Ahuja P, Sdek P, MacLellan WR (2007) Cardiac myocyte cell cycle control in development, disease, and regeneration. *Physiol Rev* 87:521–544.
6. Pendergast AM (2002) The Abl family kinases: mechanisms of regulation and signaling. *Adv Cancer Res* 85:51–100.
7. Li B, et al. (2000) Mice deficient in Abl are osteoporotic and have defects in osteoblast maturation. *Nat Genet* 24:304–308.
8. Schwartzberg PL, et al. (1991) Mice homozygous for the ablm1 mutation show poor viability and depletion of selected B and T cell populations. *Cell* 65:1165–1175.
9. Tybulewicz VL, Crawford CE, Jackson PK, Bronson RT, Mulligan RC (1991) Neonatal lethality and lymphopenia in mice with a homozygous disruption of the c-abl proto-oncogene. *Cell* 65:1153–1163.
10. Toyofuku T, et al. (2004) Guidance of myocardial patterning in cardiac development by Sema6D reverse signalling. *Nat Cell Biol* 6:1204–1211.
11. Kerkela R, et al. (2006) Cardiotoxicity of the cancer therapeutic agent imatinib mesylate. *Nat Med* 12:908–916.
12. Pye SM, et al. (2008) The effects of imatinib on pregnancy outcome. *Blood* 111: 5505–5508.
13. Swynghedauw B (1999) Molecular mechanisms of myocardial remodeling. *Physiol Rev* 79:215–262.
14. Rajabi M, Kassiotis C, Razeghi P, Taegtmeyer H (2007) Return to the fetal gene program protects the stressed heart: a strong hypothesis. *Heart Fail Rev* 12:331–343.
15. Zhu J, Wang JY (2004) Death by Abl: a matter of location. *Curr Top Dev Biol* 59: 165–192.
16. Wen ST, Jackson PK, Van Etten RA (1996) The cytostatic function of c-Abl is controlled by multiple nuclear localization signals and requires the p53 and Rb tumor suppressor gene products. *EMBO J* 15:1583–1595.
17. Agah R, et al. (1997) Gene recombination in postmitotic cells. Targeted expression of Cre recombinase provokes cardiac-restricted, site-specific rearrangement in adult ventricular muscle in vivo. *J Clin Invest* 100:169–179.
18. Henson M, et al. (2000) Insulin-like growth factor-binding protein-3 induces fetalization in neonatal rat cardiomyocytes. *DNA Cell Biol* 19:757–763.
19. Mikhailov AT, Torrado M (2008) The enigmatic role of the ankyrin repeat domain 1 gene in heart development and disease. *Int J Dev Biol* 52:811–821.
20. Shi-Wen X, Leask A, Abraham D (2008) Regulation and function of connective tissue growth factor/CCN2 in tissue repair, scarring and fibrosis. *Cytokine Growth Factor Rev* 19:133–144.
21. Gertler FB, Bennett RL, Clark MJ, Hoffmann FM (1989) Drosophila abl tyrosine kinase in embryonic CNS axons: a role in axonogenesis is revealed through dosage-sensitive interactions with disabled. *Cell* 58:103–113.
22. Gertler FB, Doctor JS, Hoffmann FM (1990) Genetic suppression of mutations in the Drosophila abl proto-oncogene homolog. *Science* 248:857–860.
23. Goga A, et al. (1995) p53 dependent growth suppression by the c-Abl nuclear tyrosine kinase. *Oncogene* 11:791–799.
24. Sawyers CL, McLaughlin J, Goga A, Havlik M, Witte O (1994) The nuclear tyrosine kinase c-Abl negatively regulates cell growth. *Cell* 77:121–131.
25. Lin J, Arlinghaus R (2008) Activated c-Abl tyrosine kinase in malignant solid tumors. *Oncogene* 27:4385–4391.
26. Plattner R, Kadlec L, DeMali KA, Kazlauskas A, Pendergast AM (1999) c-Abl is activated by growth factors and Src family kinases and has a role in the cellular response to PDGF. *Genes Dev* 13:2400–2411.
27. Gu JJ, Ryu JR, Pendergast AM (2009) Abl tyrosine kinases in T-cell signaling. *Immunol Rev* 228:170–183.
28. Kozar K, et al. (2004) Mouse development and cell proliferation in the absence of D-cyclins. *Cell* 118:477–491.
29. Pasumarthi KB, Nakajima H, Nakajima HO, Soonpaa MH, Field LJ (2005) Targeted expression of cyclin D2 results in cardiomyocyte DNA synthesis and infarct regression in transgenic mice. *Circ Res* 96:110–118.
30. Soonpaa MH, et al. (1997) Cyclin D1 overexpression promotes cardiomyocyte DNA synthesis and multinucleation in transgenic mice. *J Clin Invest* 99:2644–2654.
31. Noren NK, Foos G, Hauser CA, Pasquale EB (2006) The EphB4 receptor suppresses breast cancer cell tumorigenicity through an Abl-Crk pathway. *Nat Cell Biol* 8: 815–825.
32. Gerety SS, Wang HU, Chen ZF, Anderson DJ (1999) Symmetrical mutant phenotypes of the receptor EphB4 and its specific transmembrane ligand ephrin-B2 in cardiovascular development. *Mol Cell* 4:403–414.